

# Effects of Inertia, Load Damping and Dead-Bands on Frequency Histograms and Frequency Control of Power Systems

Davide del Giudice, *IEEE Student Member*, Angelo Brambilla, *IEEE Member*, Samuele Grillo, *IEEE Senior Member* and Federico Bizzarri, *IEEE Senior Member*

**Abstract**—The increasing penetration of renewable energy sources has been leading to the progressive phase out of synchronous generators, which constitute the main source of frequency stability for electric power systems. In the light of these changes, over the past years some power systems started to exhibit an odd frequency distribution characterised by a bimodal behavior. This results in an increased wear and tear of turbine governors and, in general, in degraded frequency performances. This is a cause of concern for grid operators, which have become increasingly interested in understanding the factors shaping frequency distribution. This paper explores the root causes of unwanted frequency distributions. The influence of some main aggregate system parameters on frequency distribution is detailed. The paper also shows that the implementation of the so-called synthetic inertia can lead to a robust unimodal frequency distribution.

**Index Terms**—Dead-band, frequency control, frequency fluctuations, load damping, low-inertia grids, synthetic inertia.

## I. INTRODUCTION

In electric power systems, frequency is the most important parameter that transmission system operators (TSOs) must control and manage, trying to limit its variations within strict bounds. Several corporations, such as for example the North American Electric Reliability Corporation (NERC), prepared documents concerning the decreasing trend in frequency quality of a complex power system. They proposed some counteractions and remedies to solve this issue, e.g., new settings for traditional generators deadbands and droop gains, demand response, the introduction of load and generation aggregators, the intervention of thermostatically controlled loads [1]–[3].

There is a quite large consensus that the main reason leading to this trend is the continuous reduction of system inertia, which is primarily due to the increasing penetration of renewable energy sources (RES) and of converter-connected loads. The focus is on these components since they deliver/absorb power independently from frequency variations, thereby constituting frequency-independent generators/loads. The general indication is that the system inertia has to be restored in some way as the number of conventional synchronous generators are replaced by RES. For instance,

this could be done by implementing the so-called synthetic inertia in converter-connected elements, which allows to mimic the frequency response of synchronous generators following power imbalances.

While on the one hand the factors determining the frequency behavior following a power disturbance are already well established, on the other hand the analysis of the parameters shaping power system frequency distribution due to the presence of stochastic load variations is still at an early stage of research. Frequency measurement data of power systems are publicly available [4] and often show that frequency distributes around its nominal value in a way that leads to *bimodal* histograms. These histograms are characterised by two frequency occurrence peaks, often located almost symmetrically around the nominal frequency value [5]–[7].

### A. Contributions

We investigate and identify the reasons that lead to unwanted frequency distributions such as for example bimodal frequency histograms. This is initially done in an analytic way through a formal approach applied to a simplified, *linear* power system model comprising a stochastic load, which constitutes the source of power mismatches [8]. We then use a modified version of the well known IEEE 14 BUS power system as a paradigm. Detailed numerical simulations are performed to compute frequency distributions in different operating scenarios. When possible, results are compared with experimental measurements of more complex power systems.

Some considerations and guidelines on how to act on power systems to avoid a bimodal frequency distribution are proposed. These considerations take into account effects due to: dead-bands of turbine governors (TGs), automatic generation control (AGC), inertia of synchronous generators, variability and stochastic characteristics of loads and generation, elements with a power versus frequency dependence (e.g., frequency-dependent loads) and possibly synthetic inertia.

The main results we show are: (i) simply increasing or restoring inertia without considering the aggregate value of the load damping parameter can be ineffective. This is in contrast to the common belief that an increase in inertia is beneficial per se. (ii) bimodal frequency distribution histograms are due to at least two very different reasons. The former is an inappropriate procedure to aggregate frequency samples [7]. The latter is due to the adoption of ineffective dead-bands, as well as of an unsuitable choice of the values of

Davide del Giudice, Angelo Brambilla, Samuele Grillo, and Federico Bizzarri are with DEIB, Politecnico di Milano, p.zza Leonardo da Vinci 32, I-20133 Milano, Italy. E-mails: {federico.bizzarri}@polimi.it.

Federico Bizzarri is also with the Advanced Research Center on Electronic Systems for Information and Communication Technologies E. De Castro (ARCES), University of Bologna, I-41026 Bologna, Italy.

other system parameters, which lead to a continuous wear and tear of TGs and to poorly-controlled swings following long-term, small power imbalances. (iii) The introduction of adequate controllers in electronically-connected loads and RES generation can sensibly and beneficially modify the aggregate values of system parameters and mainly load damping and inertia. We show that this leads to very narrow unimodal frequency distributions.

## B. Paper organisation

The paper is organized as follows. In Section II a stochastic load model is introduced. The statistical properties of a simplified power system model with a stochastic load are derived. Section III introduces the simulation environment that we use to describe how frequency distribution due to the presence of a stochastic load varies with the main system aggregate parameters, such as the load damping coefficient and inertia. In Section IV we show what happens when dead-bands are introduced in the transfer functions of TGs. Section V considers the impact of system inertia on frequency distribution. In Section VI, a photovoltaic (PV) power plant connected to the grid through a power electronic converter implementing synthetic inertia is considered and its effect on frequency distribution is analysed. Section VII resumes the main results of this work and provides some closing remarks.

## II. SIMPLIFIED MODEL OF A POWER SYSTEM WITH STOCHASTIC LOAD

Let's assume to have a simplified and linear power system model. In such a system, we consider  $\Delta\omega$  as the deviation from 1 [pu] of the angular frequency of the center of inertia (COI). We model it through the swing equation

$$2H\dot{\Delta\omega} = -D_L\Delta\omega - \eta(t), \quad (1)$$

where  $H$  is the inertia of the COI and  $D_L$  is the load damping coefficient. We assume that the  $\eta(t)$  power fluctuations in the swing equation are due to a stochastic load, modeled by the linear stochastic differential equation

$$d\eta = (\mu - \alpha\eta(t))dt + b dW_t, \quad (2)$$

where  $\alpha$  is known as the reciprocal of the reversal time,  $b$  governs the variance of  $\eta(t)$  and  $W_t$  is a scalar Wiener process.

Equations (1) and (2) can be written in compact form as

$$\begin{bmatrix} d\Delta\omega \\ d\eta \end{bmatrix} = \begin{bmatrix} 0 \\ \mu \end{bmatrix} dt - \begin{bmatrix} \frac{D_L}{2H} & \frac{1}{2H} \\ 0 & \alpha \end{bmatrix} \begin{bmatrix} \Delta\omega \\ \eta \end{bmatrix} dt + \begin{bmatrix} 0 \\ b \end{bmatrix} dW_t. \quad (3)$$

The above equation belongs to the general class of multi-dimensional linear stochastic equations in the form [9]

$$\begin{aligned} dx &= (\boldsymbol{\mu}(t) - \mathbf{A})\mathbf{x} dt + \mathbf{B} d\mathbf{W}_t \\ \mathbf{x}(t_0) &= \mathbf{x}_o, \end{aligned} \quad (4)$$

where  $\mathbf{W}_t$  is an  $M$ -dimensional Wiener process,  $\mathbf{A} \in \mathbb{R}^{N \times N}$ ,  $\mathbf{B} \in \mathbb{R}^{N \times M}$  are constant matrices,  $\boldsymbol{\mu}(t)$  is an  $N$ -dimensional vector of time functions, and  $\mathbf{x}_o$  is the initial condition. Equation (4) admits the solution

$$\mathbf{x}(t) = e^{-\mathbf{A}(t-t_0)}\mathbf{x}_o + \int_{t_0}^t e^{-\mathbf{A}(t_0-s)}(\boldsymbol{\mu}(s)ds + \mathbf{B}d\mathbf{W}_s), \quad (5)$$

and

$$\mathbb{E}[\mathbf{x}(t)] = e^{-\mathbf{A}(t-t_0)} \left( \mathbb{E}[\mathbf{x}_o] + \int_{t_0}^t e^{-\mathbf{A}(t_0-s)} \boldsymbol{\mu}(s) ds \right). \quad (6)$$

Without loss of generality, in the following we assume  $t_0 = 0$  and  $\mathbb{E}[\mathbf{x}_o] = 0$ .

The covariance matrix of  $\mathbf{x}(t)$  is the solution of the

$$\dot{\mathbf{w}} = -(\mathbf{A}\mathbf{w} + \mathbf{w}\mathbf{A}^T) + \mathbf{B}\mathbf{B}^T \quad (7)$$

differential equation (the  $^T$  super-script means transposition).

In our analysis, we focused on (4) letting both  $\mu$  constant and  $\mu(t) = \rho \sin(\Psi t)$ . In the first case, (2) models the evolution of the Ornstein-Uhlenbeck process [10], which is exponentially-autocorrelated and normally-distributed, with  $\mathbb{E}[\eta(t)] = \mu/\alpha + (\eta(0) - \mu/\alpha)e^{-\alpha t}$  time-varying mean and

$$\text{Var}[\eta(t)] = \frac{b^2}{2\alpha} (1 - e^{-2\alpha t}) \quad (8)$$

time-varying variance.  $\eta(t)$  asymptotically tends to  $\mu/\alpha \in \mathbb{R}$  as  $t$  tends to infinity. Since, in particular, we assume  $\mu = 0$ , as far as  $\alpha t \gg 0$  the stochastic load on average does not contribute power and  $\mathbb{E}[\Delta\omega]_{\alpha t \gg 0}$  is null too.

In the second case  $\mu(t)$  is used to model a slowly-varying deterministic and periodic (daily) power imbalance. We assume  $\Psi \ll 2\pi\alpha$ , viz. the period of  $\mu(t)$  is much more larger than the process reversal-time. By exploiting (6) with  $2H\alpha \neq D_L$  we get

$$\begin{aligned} \mathbb{E}[\Delta\omega] &= ke^{-\frac{D_L}{H}t} + \frac{\rho\Psi e^{-\alpha t}}{(\alpha^2 + \Psi^2)(2H\alpha - D_L)} + \\ &+ \rho_c \cos(\Psi t) + \rho_s \sin(\Psi t) \end{aligned}, \quad (9)$$

where

$$\begin{aligned} \rho_c &= \frac{\rho\Psi(2H\alpha + D_L)}{(4H^2\Psi^2 + D_L^2)(\alpha^2 + \Psi^2)} \\ \rho_s &= \frac{\rho(2H\Psi^2 - \alpha D_L)}{(\alpha^2 + \Psi^2)(4H^2\Psi^2 + D_L^2)} \end{aligned}$$

and  $k$  is chosen to guarantee that  $\mathbb{E}[\Delta\omega(0)] = 0$ . Solving (7) the expression of the variance of  $\Delta\omega$  turns out to be

$$\text{Var}[\Delta\omega] = \sigma^2 \left( 1 - \kappa_1 e^{-\frac{D_L}{H}t} + \kappa_2 e^{-\frac{D_L + 2H\alpha}{2H}t} \right) - \kappa_3 e^{-2\alpha t}, \quad (10)$$

where

$$\sigma = \frac{b}{\sqrt{2\alpha D_L(D_L + 2H\alpha)}} \quad (11)$$

and

$$\begin{aligned} \kappa_1 &= \frac{2H\alpha(D_L + 2H\alpha)}{(D_L - 2H\alpha)^2} \\ \kappa_2 &= \frac{8H\alpha D_L}{(D_L - 2H\alpha)^2} \\ \kappa_3 &= \frac{b^2}{2\alpha(D_L - 2H\alpha)^2}. \end{aligned}$$

An important aspect is that  $\boldsymbol{\mu}(t)$  does not appear in (7), thus  $\mathbf{w}(t)$  does not depend on it. Consequently, (11) is invariant w.r.t.  $\boldsymbol{\mu}(t)$ .

When  $t$  is sufficiently large, (9) and (10) simplify as

$$\mathbb{E}[\Delta\omega]_{\alpha t \gg 0} \simeq \rho_c \cos(\Psi t) + \rho_s \sin(\Psi t), \quad (12)$$

viz. a periodic function with period equal to  $2\pi/\psi$ , and

$$\text{Var}[\Delta\omega]_{\alpha t \gg 0} \simeq \sigma^2. \quad (13)$$

By observing  $\sigma$  in (11), we see that it is a constant which inversely depends on the  $D_L$  load damping, on the  $1/\alpha$  load reversal time, and on the  $H$  inertia. It is worth pointing out that the  $H$  inertia is multiplied by  $\alpha$  at the denominator of  $\sigma$  and then by  $D_L$ . This means that *the smaller  $D_L$ , the lower the effectiveness of inertia in limiting frequency deviations*. This is somewhat surprising and in contrast to the common idea that an increment of the overall system inertia is beneficial, regardless of the value of other aggregate system parameters. We will consider this matter in further detail in the following.

Another aspect is that  $D_L$  adds to  $2H\alpha$  and it is thus deemed to play a significant role in limiting frequency variations. In the light of this,  $D_L$  could be increased by exploiting thermostatically controlled loads that link frequency variations to the absorbed power [11]–[15], as well as load damping and synthetic inertia, which require a suitable implementation of RES generation and storage systems [16]–[18].

We pay now some more attention on  $\sigma$ . As  $D_L$  tends to 0,  $\sigma$  increases, i.e., the distribution of  $\Delta\omega$  around 0 flattens and extends. Thus, as shown in the following, the reduction of  $D_L$  leads to an increased probability of crossing the dead-bands implemented in TGs.

The variance of  $\Delta\omega$ , in the extreme case when  $D_L = 0$ , is

$$\text{Var}[\Delta\omega]_{D_L=0} = \frac{b^2}{4H^2\alpha^2} \left[ t + \frac{1}{\alpha} \left( 2e^{-\alpha t} - \frac{1}{2}e^{-2\alpha t} - \frac{3}{2} \right) \right]. \quad (14)$$

This expression clearly shows that  $\text{Var}[\Delta\omega]_{D_L=0}$  increases with time. As a consequence, the probability that dead-bands are crossed increases with time too. When  $t$  is sufficiently large so that  $\alpha t$  is far larger than 0, the two exponential terms in (14) are practically 0 and

$$\text{Var}[\Delta\omega]_{D_L=0, \alpha t \gg 0} \simeq \frac{b^2}{4H^2\alpha^2} \left( t - \frac{3}{2\alpha} \right). \quad (15)$$

This means that, at least in the simplified model of the power system, if  $D_L = 0$ , by acting on the system inertia alone, the frequency is likely to trespass the bounds of the TGs. This is the first relevant result of the paper.

### III. NUMERICAL SIMULATION SETUP

The simplified model described by (3) may only grab the main features of a complex non-linear power system model. Thus, we resort to numerical simulations and elect the well known IEEE 14 BUS power system to the role of our benchmark. It is extended with several additions, that are used in different ways and scenarios depending on the factors shaping frequency deviations that we want to highlight.

- Each of the two generating units of the IEEE 14 BUS power system is equipped with a TG, whose control scheme is modified by including a dead-band block (see Fig. 1). Dead-bands are enabled/disabled according to the specific features that simulations aim at highlighting. As is well known, dead-bands are implemented to prevent them from relentlessly operating even following small

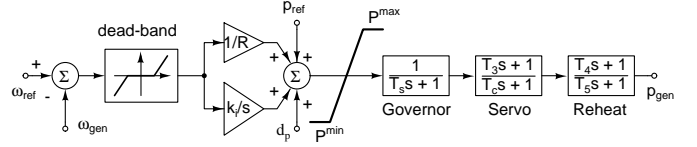


Fig. 1. Schematic of a TG with dead-band. The value  $d_{za}$  corresponds to the frequency threshold above which the TG modifies the generator power output.

power variations. In principle, this insertion should not degrade the almost-Gaussian distribution of frequency around the nominal value.

- An additional stochastic load is connected to BUS13.

It is modeled as [8]  $p_L(t) = \eta(t) P_{L0} \left( \frac{|v(t)|}{V_0} \right)^\gamma$ , where  $P_{L0}$  is the nominal active power of the load,  $V_0$  is the load voltage rating,  $v(t)$  is the bus voltage at which the load is connected,  $\gamma$  governs the dependence of the load on bus voltage [19]. Load active power is ruled by the  $\eta(t)$  Ornstein-Uhlenbeck's process in (2) with  $\eta(0) = 0$ ,  $\alpha = 0.5$ ,  $b = 1$ ,  $\mu = 0$  [8]<sup>1</sup>. This choice leads to a stochastic load that on average does not absorb active power. The purpose of this set-up to stimulate the power system and its controllers with a continuous active power disturbance. Two different values of  $P_{L0}$ , namely 1 MW and 10 MW, are considered.

- The conventional load of the IEEE 14 BUS system connected at BUS13, which has  $P_{D0} = 14.9$  MW nominal power, is replaced by the daily time-varying load<sup>2</sup>

$$p_D(t) = P_{D0} (1 + \Delta p_D(t)) \left( \frac{|v(t)|}{V_0} \right)^\gamma,$$

where

$$\Delta p_D(t) = -0.12 \sin \left( \frac{t}{24 \times 3600} \right) [\text{pu}]. \quad (16)$$

In the conventional IEEE 14 BUS without dead-bands, the addition of this daily time-varying load causes the corresponding slow intervention of the TGs to balance the power mismatch. Frequency deviates from its nominal value of a very small amount due to the overall low power variation of the drifting load. As shown in the following, the effect of this drifting load on frequency distribution significantly changes when dead-bands are introduced.

- To compensate the slowly daily drifting power, we introduce a simple AGC model as described in [6], [20]. The TG of generator G2 in the IEEE 14 BUS test system is driven by a simple AGC described by the equation  $\dot{P}_{agc} = k_{agc} (1 - \omega_{acg})$ . In our implementation  $\omega_{acg}$  is the angular frequency of the COI and the AGC output  $P_{agc}$  drives the  $d_p$  terminal of the summation block of the TG schematic shown in Fig. 1.

The choice of adequate AGC parameters and TGs dead-bands to avoid wear and tear may be a difficult task [5]. In any case, regardless of dead-bands, the action of the AGC

<sup>1</sup> Typically, the  $\alpha$  parameter ranges from  $1/20$  to  $1/2$  [7], [8].

<sup>2</sup> A similar version of power drifting was already used in [6].

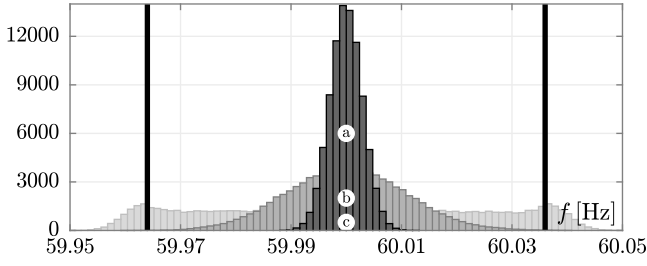


Fig. 2. The ① histogram shows the frequency deviations at nominal conditions and parameters of the IEEE 14 BUS power system. The ② histogram refers to the case with dead-bands and the ③ one refers to the case with dead-bands and with  $D_L = 0$ . Vertical lines show the  $d_{za}$  frequency limits of the dead-band (see Fig. 1). All histograms are displayed with an equal number of bins (same width). Histograms report the number of occurrences in each bin. The value of  $P_{L0}$  is 1 MW.

should be very slow and immune from fast frequency fluctuations due to stochastic loads with relatively short reversal time as in our case.

In every simulated scenario we always performed an eigenvalue analysis after the computation of the power-flow solution to assess whether the modified system remained stable in spite of the additions above [19]–[21].

We also assume that the modified IEEE 14 BUS power system is ergodic, stationary or cyclo-stationary. The Ornstein-Uhlenbeck’s process can be assumed stationary or cyclo-stationary if we consider its behavior for  $\alpha t \gg 0$ , as we do in all scenarios. Ergodicity allows us to substitute a set of relatively short time-domain simulations with a single long lasting time-domain simulation to derive statistical properties.

In the various scenarios we simulate the IEEE 14 BUS power system for at least 24 hours after a sufficiently large set-up time interval. We pick a frequency sample every 1 s, thereby collecting  $3600 \times 24 = 86400$  samples of the frequency variations of the rotor speed of synchronous generators. Such samples are organised in histograms.

#### IV. FREQUENCY DEVIATIONS

To have a reference scenario for frequency deviations and to allow further easy comparisons, we firstly simulate the nominal IEEE 14 BUS system by adding the stochastic load only. The histogram of frequency deviations obtained in that case is reported in Fig. 2 [①]. The continuous intervention of the TGs regulating the mechanical power from the prime movers that drive the two synchronous generators keeps frequency well inside the dead-bands, whose thresholds are identified by vertical red dashed lines in Fig. 2. The result is excellent also due to the modest variance of the stochastic load. The frequency deviations with  $P_{L0} = 10$  MW are still limited and are thus not reported.

##### A. TG with dead-bands

As it is well known, dead-bands are inserted in the controllers of TGs to limit their wear and tear. We thus set up a new scenario that adds dead-bands to TGs by setting  $d_{za} = 720 \times 10^{-6}$  [pu] (36 mHz) in the block shown in the schematic of Fig. 1. This value is compliant with the standards

in [22]. We simulate the power system for 24 hours and also in this scenario almost all of frequency deviation occurrences lay inside the dead-band (see the ② histogram in Fig. 2).

An interesting result is the ③ histogram shown in Fig. 2. It is obtained with dead-bands and with  $D_L = 0$ , i.e., by fictitiously assuming no dependence of the load power from frequency as if, for example, each induction motor were equipped with an electronic controller that decouples it from the grid. We see an almost flat portion of the histogram inside the dead-band as predicted by (13) and (14). There is a modest increase of occurrences just outside the dead-band where the power fluctuations activate the TGs. When frequency exceeds the dead-band, TGs activate and pull frequency back. We recall that the power-flow solution in normal operating conditions gives a total active power absorbed by loads equal to 259 MW. When we set  $P_{L0} = 1$  MW, this value is about 0.4% of the total active load power. This power variation, albeit small, leads to frequency fluctuations that are sufficiently large to trigger the intervention of TGs. Since we use the low-pass filtered white Gaussian source with variance given by 8 (recall that we set  $b = 1$  and  $\alpha = 0.5$ ) we tested the stability of the IEEE 14 BUS power system with a maximum power variation of  $\pm 5P_{L0} = \pm 50$  MW. This corresponds to the  $\text{erf}\left(\frac{5}{\sqrt{2}}\right) \simeq 1 - 5.7330 \times 10^{-7}$  expected fraction of the generated samples that fall inside the  $\pm 5P_{L0}$  interval. Our expectation is that the IEEE 14 BUS power system almost always works in a stable condition.

The first consideration about the ③ histogram is that *the complete elimination of any dependence of the power from frequency, i.e., the setting of  $D_L = 0$ , defeats the purpose of inserting dead-bands to limit wear and tear of TGs*. As anticipated, we stress that an unaware and independent selection of the dead-band settings from the aggregate  $D_L$  value of a power system might be useless.

The second consideration is that frequency distribution greatly deteriorates. We see that the shape of the histogram largely differs from a Gaussian one. Coherently with (13), we state that *frequency deterioration can not be effectively compensated by acting on the  $H$  inertia of the system if  $D_L$  is too low. This deterioration further aggravates as the stochastic load variation increases*. To enforce this statement, we repeat the last simulation with a higher  $P_{L0}$  value (10 MW), corresponding to about 4% of the total nominal load power. We expect larger occurrences of frequency deviations outside the dead-bands and mainly more interventions of TGs. The frequency histogram corresponding to this scenario is reported in Fig. 3 [④]. It highlights the presence of a *bimodal* frequency distribution [6], characterised by two symmetric peaks of frequency occurrences located just outside the dead-bands, where TGs start to counteract frequency deviations. Such occurrences increase with the variance of the stochastic load. Therefore, an adequately large variance might result in bimodal frequency histograms even if  $D_L \gg 0$ .

##### B. Bimodal histograms

In computing the results of previous scenarios we have assumed that dead-bands equally extends from the 60 Hz

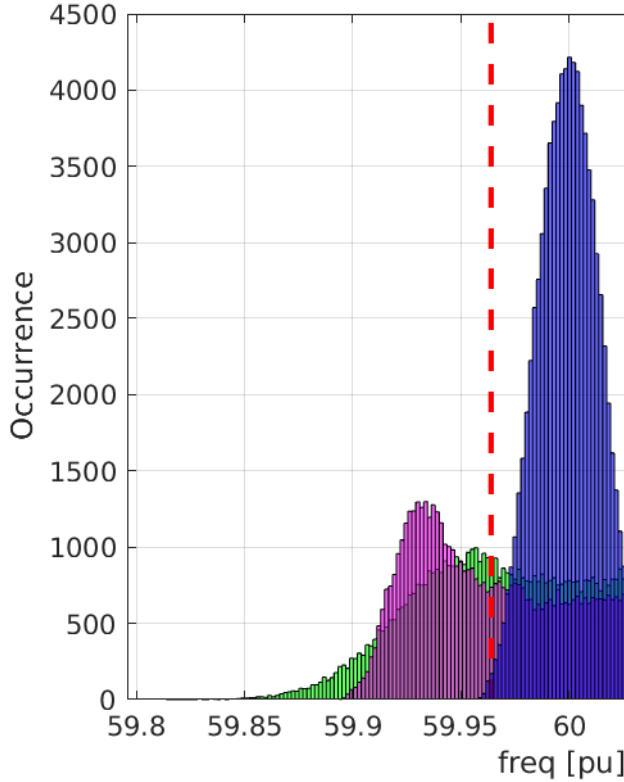


Fig. 3. ⓐ histogram:  $d_{za} = 36$  mHz,  $D_L = 0$  and  $P_{L0}$  is 10 MW. ⓑ histogram:  $D_L = 2.0$ ,  $d_{za} = 100$  mHz  $P_{L0} = 1$  MW, power drifting is introduced (see Eq. (16)). The ⓐ and ⓑ histograms are bimodal. The ⓒ histogram refers to the same scenario of the ⓑ one but with the introduction of the AGC ( $k_{agc} = 0.01$ ) that drives the TG of the G2 generator and with  $d_{za} = 36$  mHz. Vertical lines mark the extension of the dead-band corresponding to the ⓐ and ⓒ histograms.

center frequency. Said in the opposite way, we have assumed that the average value of frequency is 60 Hz and thus it locates exactly in the mid-point of the dead-band. We now introduce the deterministic load power drift described by (16), namely we assume that the load at BUS13 slowly varies during the 24 hours along which we simulate the IEEE 14 BUS power system. This power imbalance causes a corresponding frequency shift.

By considering our simplified power system model and the daily time-varying load, Eq. (12) and Eq. (13) show that the average value of  $\Delta\omega$  periodically cycles around 0 with a constant  $\sigma$  variance, i.e., the central Gaussian curve in Fig. 4 shifts horizontally back and forth over time. If the average frequency variation and  $\sigma$  are large enough, we expect that the probability of crossing the dead-band increases cyclically. The result will be a bimodal histogram with equal peaks of occurrences outside of the dead-band. We simulated the system with  $D_L = 2$ ,  $d_{za} = 100$  mHz, i.e., with a larger dead-band, and  $P_{L0} = 1$  MW, thereby obtaining the ⓒ frequency histogram shown in Fig. 3. It can be noticed that no AGC was introduced to compensate the slowly varying deterministic power. As a consequence, the average frequency value varies in a slow (quasi-static) manner above and below 60 Hz. This translates into going closer to the upper and lower limits of the

dead-band. Thus, as already stated, the likelihood of crossing the dead-band and triggering the activation of TGs increases.

We underline that the ⓐ and ⓒ histograms are obtained in two different scenarios. In the former we have a too low (i.e.,  $D_L = 0$ ) load damping and in the latter we have a poorly managed, slow varying power imbalance. Although the power systems characteristics and setups of the two scenarios are very different, they both result in bimodal histograms.

### C. bimodal frequency histograms of the Great Britain's grid

Let us now consider a real situation, namely the frequency histogram of the Great Britain grid displayed from data recorded along June 2018. Also in this case the frequency samples were picked every 1s as in our simulations. The related histogram is depicted in Fig. 5. It refers to the *entire month of June*. It can be clearly seen that it has a bimodal shape. Our rhetorical question is: “Which kind of bimodal histogram is it?” Better said: “Is it of type ⓐ (too small  $D_L$ ) or ⓒ (inadequately handled daily power imbalance)?” The answer comes if we observe the hourly frequency histograms of the Great Britain grid for example in June 1<sup>st</sup>, 2018. Analogous results are obtained by considering other days. Each hourly histogram seems *unimodal* and none of them clearly shows any neat bimodal shape. The histograms shown in Fig. 6 highlight that there is a daily frequency drift possibly due to a mismatch of power demand and planned generation not adequately corrected by AGCs and that there is some sort of dead-band (i.e., 100 mHz, corresponding to the same dead-band setting adopted in the ⓒ histogram of Fig. 3) that keeps primary frequency regulation inside the dead-bands. The shapes of the hourly and daily histograms suggest that there may be an adequate level of load damping ( $D_L$ ) introduced by frequency dependent loads.

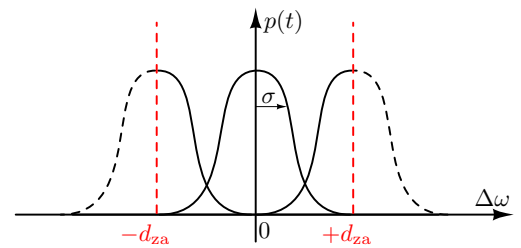


Fig. 4. Qualitative effect of the daily time-varying load on frequency distribution when AGC is absent ( $p(t)$  denotes probability).

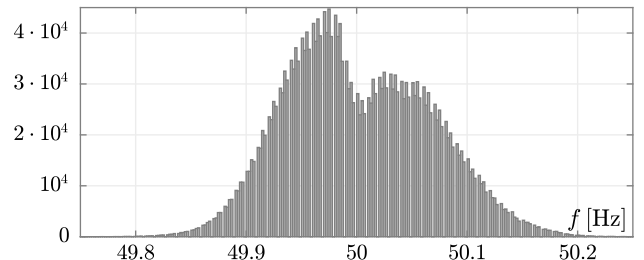


Fig. 5. Frequency histogram of the Great Britain grid, June 2018.

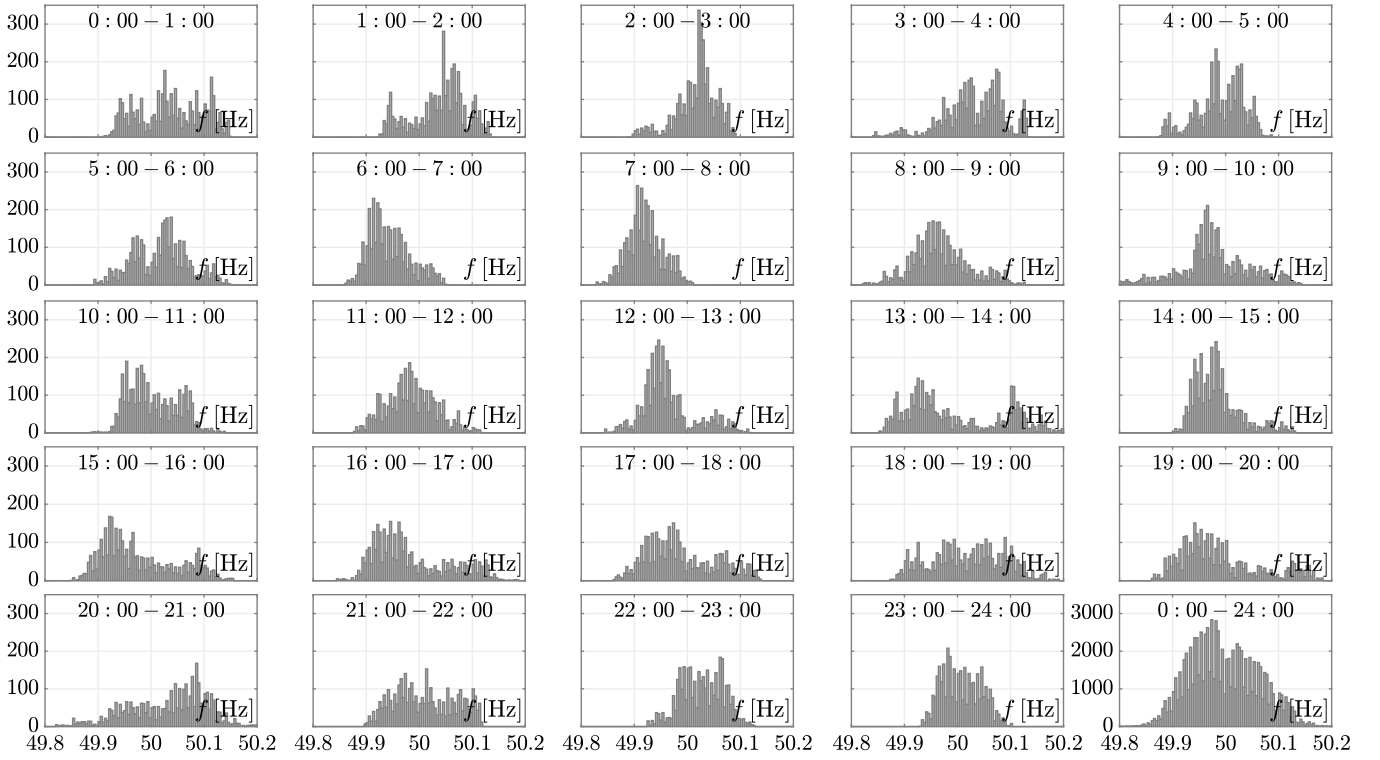


Fig. 6. Frequency histograms of the Great Britain grid, June 1<sup>st</sup>, 2018. Histograms display occurrences of frequency deviations on an hourly basis. The histogram in the lower-right corner considers the samples of the entire day.

In the monthly histogram of Fig. 5 there is an excess of occurrences due to a lack of power production with respect to power demand that leads to the asymmetry of the two peaks below and above 50 Hz. The number of occurrences below 50 Hz exceeds those above. We are aware that our statements are a long shot at best, since we do not have detailed information about the characteristics of the Great Britain grid. However we dare say that *monthly frequency samples aggregates may not constitute a valid indicator of the true nature (i.e., unimodal or bimodal) of power system frequency. Thus, conclusions drawn “tout court” from them could be misguided.* For instance, in the case of Great Britain’s grid, a seemingly bimodal monthly frequency histogram could be due to the sum of unimodal hourly histograms collected in a power system prone to a daily frequency drift.

The correct aggregation window for frequency samples depends on power system characteristics. In our scenarios an hourly window should be adequate, since it is a time interval large enough with respect to typical power system time constants to collect a sufficient number of samples (ergodic process), but short enough compared to the slow drifting load dynamics. The same seems true for the Great Britain’s case.

Another aspect worth further discussing is that the insertion of dead-bands does not limit wear and tear of TGs if the frequency drifting is not properly compensated and the frequency equilibrium point (short term average frequency) is not kept as close as possible to the nominal value.

#### D. Automatic generation control

The frequency drifting caused by the daily variation of the load/generation imbalances can be compensated by a well designed AGC. In order to address this issue, we insert in the IEEE 14 BUS power system the simple AGC model described in Section III. The transfer function of the AGC is made up of a single pole in the frequency origin. Its gain has to be set so that it counteracts the hourly frequency variation caused by the deterministic drifting load, while practically filtering out the fast fluctuations due to the stochastic load.

We repeat the simulation of the scenario with the daily variable load but with narrower dead-bands. The result obtained by simulating this scenario with the  $D_L = 2.0$ ,  $d_{za} = 36$  mHz and  $P_{L0} = 1$  MW parameters is given by the ④ histogram depicted in Fig. 3. It is immediate to appreciate that the AGC largely compensates for the deterministic power drift. The ④ histogram is completely different from the other two in the same figure and resembles the shape of a Gaussian probability density function that adequately lays inside the dead-band.

This result has suggested our comments on the daily histograms of the Great Britain’s grid, i.e., that there may be a poor compensation of even small power imbalances which leads to a bimodal monthly frequency histogram.

## V. INERTIA

In presenting the frequency histograms obtained in the scenarios considered so far, we have not explicitly paid attention to the system inertia. Better said, we kept fixed the  $H$  inertia

parameter of all the synchronous generators and compensators of the IEEE 14 BUS power system.

In [7] it is stated that the main factors influencing frequency distribution are load damping and TG dead-bands, while the inertia is reputed to have a minimal impact. Actually, according to (11), inertia positively influences frequency deviations, i.e., the denominator is greater than 1 and  $\sigma < b$ , if  $H \gg (1-2\alpha D_L^2)/(4\alpha^2 D_L)$ . We remark that if  $D_L^2$  is sufficiently large the right hand side of the inequality becomes negative. This means that  $H$  has a marginal role in limiting frequency deviations. Once more we underline that  $D_L$  must assume adequate values with a proper level of  $H$ , otherwise the Gaussian shape of the probability density function flattens as highlighted by the simulated scenarios of Section IV. This clearly indicates that *if the inertia of a power system decreases to due to a higher penetration of RES-fuelled converter-connected generation (and converter-connected loads), the frequency deviation can be still kept small if the value of  $D_L$  is adequately large.*

To show the influence of inertia on frequency deviations, we considered three different scenarios. In each of these scenarios we have  $d_{za} = 36$  mHz,  $P_{L0} = 1$  MW and  $D_L = 0$ . Furthermore, we do not introduce any daily time-varying load and thus there is no need to introduce AGCs.

In the first and second scenarios we multiply the  $H$  inertia of each synchronous generator and compensator by 10 times. Having in mind (14) and (15), in the first scenario the simulation lasts one day, whereas in the second scenario it lasts four days. In the third scenario we multiply by 100 the inertia, thus remarkably increasing it, and collect samples along 8 days. The increase of the simulation time interval is dictated by the fact that  $H^2$  is at the denominator in (14).

According to the common belief that inertia restoration is a must against frequency degradation, we would expect very limited frequency deviations and thus a very well shaped histogram. The three histograms corresponding to these scenarios are shown in Fig. 7. They are normalised to estimate the probability density and the bins do not count occurrences as in the previous histograms. This is done since the number of samples largely differ in these three scenarios. The main aspect that we easily see is that frequency deviates from 60 Hz with almost the same probability inside the dead-band. When the frequency exits the dead-bands, the TGs intervene to pull frequency back inside the dead-band. They constitute some sort of “barrier”. These histograms do not have at all the shape of a Gaussian centered at 60 Hz, characterised by a very small variance.

We believe that this is a relevant result that is *in contrast to the common belief that inertia must be increased independently from any other aggregate parameter of a power system to counteract the negative effects of larger penetration of RES generation.*

## VI. SYNTHETIC INERTIA

Most of RES can be regarded as stochastic sources due to the volatility of their primary energy source (e.g., wind and sun). This means that the effects of their power output

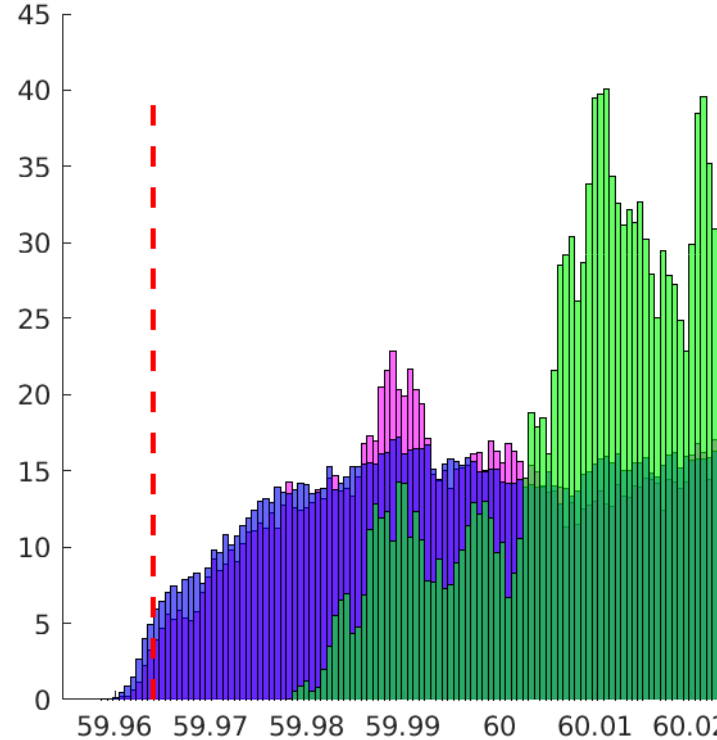


Fig. 7. The  $\textcircled{G}$  ( $10 \times H$ , 1 day),  $\textcircled{H}$  ( $10 \times H$ , 4 days) and  $\textcircled{I}$  ( $100 \times H$ , 8 days) histograms correspond to the first, second and third scenarios, respectively.  $d_{za} = 36$  mHz,  $P_{L0} = 1$  MW  $D_L = 0$ . The histograms are normalised to estimate the probability density.

variability on frequency can be considered very similar to those of the stochastic load described in the previous sections, namely, an increase of generation can be compared to a decrease in load demand and vice versa. The main difference may be related to the statistical properties of these sources.

RESs can be generally considered inertia-less for two main reasons. First, as in the case of solar plants, they lack of a mechanical rotating mass, which makes them incapable of exchanging and converting kinetic energy after a power mismatch to limit frequency variations. Second, unless synthetic inertia is implemented, such plants are typically connected to the grid through power electronic converters whose control schemes do not allow to modify their power output based on frequency fluctuations.

In this section we evaluate how frequency variations can be mitigated through the installation of an aggregated PV power plant connected to the IEEE 14 BUS power system at BUS11 by means of a converter implementing *synthetic inertia*. The word *synthetic* means that the converter controls are such that, when a power mismatch occurs, the behavior of the power plant in terms of power and energy exchange resembles that of a synchronous generator. It is worth noticing that synthetic inertia does an “endogenous” action by leveling the fluctuations of the RES and an “exogenous” action by counterbalancing the stochastic variations of external loads.

The block schematic of the PV power plant with synthetic

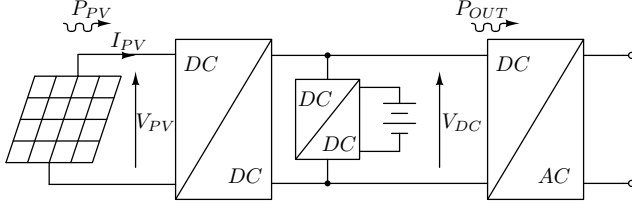


Fig. 8. Connection scheme of the PV plant and battery pack to the IEEE 14 BUS power system.  $V_{pv}^{ref} = 700V$ ,  $I_{pv}^{ref} = 2.8571kA$ ,  $V_{dc}^{ref} = 680V$ . The superscript <sup>ref</sup> denotes the reference PV plant operating conditions considered during simulation.

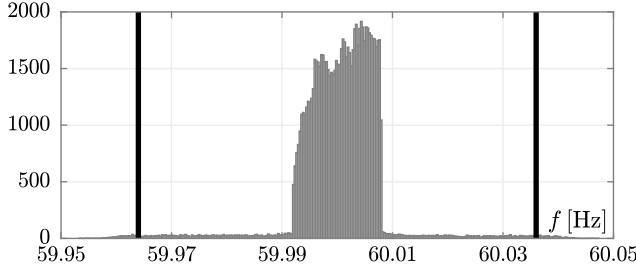


Fig. 9. The frequency histogram obtained when the PV field implementing synthetic inertia is added to the IEEE14 power system.  $D_L = 0$ ,  $P_{L0} = 1$  MW, no AGC, no power load drifting. Vertical lines correspond to the dead-band thresholds.

inertia is shown in Fig. 8. In this design we are only interested in the high-level behavior of the system and thus we acted with this target during its design. A PV field supplies power to the DC/DC converter that is equipped with a maximum power point tracker. The DC link voltage is kept constant by the DC/DC bidirectional converter connected to the battery pack. The power delivered/absorbed by the bidirectional DC/AC converter is that set by the maximum power point tracker, by the DC/DC converter and by the specific control schema that implements synthetic inertia. An important aspect in implementing the synthetic inertia controller is the maximum power that can be delivered by the DC/AC converter and the energy capacity of the storage system. In our case the peak power capacity of the PV field and of the DC/AC converter are respectively 1 and 2 MW, whereas the energy stored in the battery pack is 160 MJ. These design choices allow for power and energy variations comparable to those of the stochastic load. As consequence, on average synthetic inertia does not contribute either net power or energy.

We performed a simulation with the addition of synthetic inertia,  $D_L = 0$ ,  $P_{L0} = 1$  MW and without either daily time-varying load or AGC. The results obtained are depicted in Fig. 9. With the only exception of the presence of synthetic inertia, the simulation setup is analogous to that used to derive the histograms reported in Fig. 7. Thus, the histograms in the two figures can be compared to easily assess the significant, beneficial effect of synthetic inertia on frequency distribution. The histogram of Fig. 9 shows that almost all frequency deviations occurrences concentrate in a very small interval around 60 Hz. This happens since the reversal time of the stochastic load is 2s while the bandwidth of the

controller implementing synthetic inertia is about 1 kHz. Thus, the controller is relatively fast and efficiently manages the stochastic load by practically keeping frequency around 60 Hz.

The need for a relatively small capacity of the battery pack with respect to the very large kinetic energy stored in the full IEEE 14 BUS system is due to the fact that it can be largely and quickly exchanged with the grid even when frequency variation is small. Furthermore its action on frequency does not depend on  $D_L$ . This shows that the use of synthetic inertia may be extremely convenient and viable to control frequency fluctuations due to stochastic loads [7].

## VII. CONCLUSIONS

The first conclusion we come on is that an increase of system inertia does not lead to a Gaussian frequency distribution if the load damping does not have a proper value. This means that to keep frequency variations small and well shaped we have to simultaneously act on these two system parameters. The second conclusion is that any slow deterministic frequency drift must be compensated to avoid tear and wear of TGs. Acting on electronic controllers of load and RES is beneficial if they both increase inertia (synthetic) and load damping (synthetic).

## REFERENCES

- [1] North American Electric Reliability Corporation (NERC), *Balancing and Frequency Control*, 2011.
- [2] —, *Frequency Response Initiative Report: The Reliability Role of Frequency Response*, 2018.
- [3] Z. A. Obaid, L. M. Cipcigan, L. Abraham, and M. T. Muhssin, "Frequency control of future power systems: reviewing and evaluating challenges and new control methods," *Journal of Modern Power Systems and Clean Energy*, vol. 7, no. 1, pp. 9–25, 2019.
- [4] *National grid frequency data for 2016*, <https://www.nationalgrid.com/uk/electricity/balancing-services/frequency-response-services/firm-frequency-response?market-information>.
- [5] M. Liu, F. Bizzarri, A. M. Brambilla, and F. Milano, "On the impact of the dead-band of power system stabilizers and frequency regulation on power system stability," *IEEE Transactions on Power Systems*, vol. 34, no. 5, pp. 3977–3979, Sep. 2019.
- [6] F. M. Mele, A. Ortega, R. Zarate-Minano, and F. Milano, "Impact of variability, uncertainty and frequency regulation on power system frequency distribution," in *2016 Power Systems Computation Conference (PSCC)*, June 2016, pp. 1–8.
- [7] P. Vorobev, D. M. Greenwood, J. H. Bell, J. W. Bialek, P. C. Taylor, and K. Turitsyn, "Deadbands, droop, and inertia impact on power system frequency distribution," *IEEE Trans. on Power Systems*, vol. 34, no. 4, pp. 3098–3108, July 2019.
- [8] F. Milano and R. Zárate-Miñano, "A systematic method to model power systems as stochastic differential algebraic equations," *IEEE Trans. on Power Systems*, vol. 28, no. 4, pp. 4537–4544, Nov 2013.
- [9] L. Arnold, *Stochastic Differential Equations: Theory and Applications*. Wiley, 1974.
- [10] D. T. Gillespie, "Exact numerical simulation of the ornstein-uhlenbeck process and its integral," *Phys. Rev. E*, vol. 54, pp. 2084–2091, Aug 1996. [Online]. Available: <https://link.aps.org/doi/10.1103/PhysRevE.54.2084>
- [11] H. Zhao, Q. Wu, S. Huang, H. Zhang, Y. Liu, and Y. Xue, "Hierarchical control of thermostatically controlled loads for primary frequency support," *IEEE Transactions on Smart Grid*, vol. 9, no. 4, pp. 2986–2998, July 2018.
- [12] Z. Xu, J. Ostergaard, M. Togeby, and C. Marcus-Moller, "Design and modelling of thermostatically controlled loads as frequency controlled reserve," in *2007 IEEE Power Engineering Society General Meeting*, June 2007, pp. 1–6.
- [13] H. Hao, B. M. Sanandaji, K. Poolla, and T. L. Vincent, "Aggregate flexibility of thermostatically controlled loads," *IEEE Transactions on Power Systems*, vol. 30, no. 1, pp. 189–198, Jan 2015.

- [14] F. Baccino, F. Conte, S. Massucco, F. Silvestro, and S. Grillo, "Frequency Regulation by Management of Building Cooling Systems Through Model Predictive Control," in *2014 Power Systems Computation Conference*, 2014, pp. 1–7.
- [15] V. Trovato, I. M. Sanz, B. Chaudhuri, and G. Strbac, "Advanced control of thermostatic loads for rapid frequency response in great britain," *IEEE Transactions on Power Systems*, vol. 32, no. 3, pp. 2106–2117, May 2017.
- [16] F. Jibji-Bukar and O. Anaya-Lara, "Frequency support from photovoltaic power plants using offline maximum power point tracking and variable droop control," *IET Renewable Power Generation*, 2019.
- [17] J. Fang, P. Lin, H. Li, Y. Yang, and Y. Tang, "An improved virtual inertia control for three-phase voltage source converters connected to a weak grid," *IEEE Transactions on Power Electronics*, 2018.
- [18] J. Kim, V. Gevorgian, Y. Luo, M. Mohanpurkar, V. Koritarov, R. Hovsopian, and E. Muljadi, "Supercapacitor to provide ancillary services with control coordination," *IEEE Transactions on Industry Applications*, vol. 55, no. 5, pp. 5119–5127, 2019.
- [19] F. Milano, "A Python-based software tool for power system analysis," in *Procs. of the IEEE PES General Meeting*, Vancouver, BC, Jul. 2013.
- [20] P. Kundur, *Power system stability and control*. New York: McGraw-Hill, 1994.
- [21] F. Milano, *Power System Modelling and Scripting*. London: Springer, 2010.
- [22] North American Electric Reliability Corporation (NERC), *Frequency Response Initiative Report: The Reliability Role of Frequency Response*, 2012.